DEUTSCHES ELEKTRONEN-SYNCHROTRON

DESY 94-147
August 1994



# Summary of the Eilat Workshop

F. Sciulli
*Columbia University, New York, USA*

ISSN 0418-9833

NOTKESTRASSE 85 - 22603 HAMBURG

To be sure that your preprints are promptly included in the
HIGH ENERGY PHYSICS INDEX,
send them to (if possible by air mail):

**DESY**
**Bibliothek**
**Notkestraße 85**
**22603 Hamburg**
**Germany**

**DESY-IfH**
**Bibliothek**
**Platanenallee 6**
**15738 Zeuthen**
**Germany**

DESY 94-147
August 1994

ISSN 0418-9833

# Summary of the Eilat Workshop

Frank Sciulli
Columbia University

February 1994

**Abstract**

A review is presented of the topics discussed at the International Workshop on Deep Inelastic Scattering (DIS) and Related Subjects held in February 1994 at Eilat, Israel .

## 1 Introduction

In the beginning, there was an algebra. This $SU(3)$ contained base states called quarks [1], mathematical constructs that made predictions more transparent, but did not require "real" quarks until the discovery of *scaling* [2]. Then came QCD, and our modern paradigm for hadronic structure was born. And yet, we remember that sum rules were required by the algebra *before* there were even quarks.

It seems appropriate at this workshop celebrating structure functions, to begin with a review of the impressive body of knowledge on the constituents of nucleons gained from two decades of experiments at fixed target facilities. After reviewing sum rules, we turn to the quark densities (including spin densities), where there are some interesting new developments. Then we discuss results from HERA, including some comparisons between the published results. Finally, we discuss some subjective impressions.

We begin by reviewing the language used in deep inelastic scattering. All processes under discussion involve the scattering of a lepton ($l$) from a nucleon($N$)

$$l + N \rightarrow l' + X$$



resulting in a final-state lepton ($l'$) and an hadronic system ($X$). Experimental cross-sections from these reactions are used to extract *Structure Functions,* which describe the interactions of the relevant boson propagator with the nucleon. The structure functions specify the differential probability for finding a quark within the nucleon with a fraction of the initial nucleon momentum between $x$ and $x + dx$. In general, there can be dependence of the structure functions on the square of the four-momentum transfer ($-Q^2$) between the lepton and nucleon systems. The $Q^2$-dependence is described by the perturbative GLAP evolution equations [3], though the same equations say little explicitly about the $x$-dependence.

A few examples of the relationships between the lepton nucleon scattering cross-sections and structure functions will help to orient us[4]. For the case of photon exchange, appropriate to fixed target electron or muon scattering as well as for HERA experiments in the $(x, Q^2)$ regime available at low luminosity, the cross-section is given by

$$\frac{d^2\sigma^{ep}}{dx\ dQ^2} = \frac{2\pi\alpha^2}{xQ^4}\left[2(1-y) + \frac{y^2}{1+R}\right] F_2^{ep}(x, Q^2) \qquad (1)$$

where $R = \sigma_l/\sigma_t$ is the ratio of longitudinal to transverse cross-sections, which would be zero for scattering from stationary or collinear spin 1/2 quarks[1], but has a small but predictable magnitude in QCD. Within the naive quark model, $F_2^{eN}$ is given by a sum over all quarks involving the charges ($e_q$) and quark densities ($q$):

$$F_2^{ep} = \sum_{quarks} e_q^2 x[q(x) + \overline{q}(x)] \qquad (2)$$

The sum includes all known quark types $(u, d, s, c, ...)$. At small $x$, $F_2$ is dominated by the seas of quarks and antiquarks.

For the charged-current scattering of *neutrinos* by nucleons (averages over neutrons and protons), by contrast,

$$\frac{d^2\sigma^{\nu(\overline{\nu})N}}{dx\ dy} = \frac{G^2 s}{4\pi}\left\{\left[2(1-y) + \frac{y^2}{1+R}\right] F_2^{\nu N}(x, Q^2) \pm [y(2-y)]\, x F_3^{\nu N}(x, Q^2)\right\} \qquad (3)$$

[1]This "Callen-Gross" requirement applies in what is sometimes referred to as the *naive quark model* . Here, all effects due to binding and internal motion are neglected; structure functions are completely independent of $Q^2$.

in terms of the weak coupling, $G$, and center of mass energy, $\sqrt{s}$. The interpretations of these structure functions in the naive quark model are

$$\begin{pmatrix} F_2^{\nu N} \\ xF_3^{\nu N} \end{pmatrix} = \sum_{quarks} x[q(x) \pm \overline{q}(x)] \qquad (4)$$

which do *not* involve the quark electric charges. The integral $\int F_2^{\nu N}(x)\,dx$ represents the fraction of the total nucleon momentum carried by quarks. The experimental value of about 1/2, together with the requirement (momentum sum rule) that *all* constituent momenta must add to that of the proton, was an early indicator of the importance of gluons to nucleon structure.

The predicted ratio of $F_2^{\nu N}$ from equation (4) to $F_2^{eN}$ as described in equation (2) is the famous factor 5/18, corresponding to the mean square charge of quarks. This simple relation applies when complications arising from strange and charm quarks inside the nucleon can be neglected. The prediction is well satisfied [5] at larger values of $x$ to the level of experimental precision of normalization between neutrino and muon experiments.

The $xF_3$ structure function is rather special in that its determination, possible because of the parity violation inherent in the weak interactions, is independent of $R$. The function $xF_3$ is a direct measure of the nucleon's *valence* quark distribution and its evolution[2] with $Q^2$ in QCD is simple [6].

The spin structure of constituent quarks is determined by measuring the asymmetry in lepton-nucleon scattering between longitudinally polarized leptons and longitudinally polarized nucleons. In such experiments the asymmetry at fixed values of $(x, Q^2)$ is given by [7] [8]

$$A(x,Q^2) = \frac{d^2\{\sigma(\uparrow\downarrow) - \sigma(\uparrow\uparrow)\}}{d^2\{\sigma(\uparrow\downarrow) + \sigma(\uparrow\uparrow)\}} \approx \frac{g_1(x,Q^2)}{F_2(x,Q^2)} 2x[1 + R(x,Q^2)]$$

for scattering of a completely polarized beam lepton by a completely polarized target. [In this relation, $\sigma(\uparrow\uparrow)$ refers to the cross-section for scattering when the lepton and nucleon spin are aligned.] The *spin* structure function, $g_1$, has interpretation

$$g_1 = \frac{1}{2} \sum_{quarks} e_q^2[q^{\uparrow}(x) - q^{\downarrow}(x) + \overline{q}^{\uparrow}(x) - \overline{q}^{\downarrow}(x)]$$

[2]This *nonsinglet* nature of $xF_3$ is shared by the difference, $F_2^{ep} - F_2^{en}$, measured with charged leptons.



where, for example, $q^{\uparrow}(x)$ is the number of quarks of type $q$ with spin aligned with the lepton.

## 2 Sum Rules

Historically, the algebra underlying sum rules was the foundation for the development of Quantum ChromoDynamics (QCD). In most cases, these sum rules follow from requirements of that current algebra though they are more simply and physically viewed as consequences of the quark model. For the following four sum rules, the definitions are such that, for example, the total number of $u$-quarks in the proton is $U = \int u(x)dx$. We further make use of isospin invariance, which requires that the density distribution of $u$-quarks in the proton equals that of $d$-quarks in the neutron. There has been recent experimental activity on the last three relations, so we will proceed to discuss those more fully.

- Adler Sum Rule [9], obtained from neutrino-nucleon structure functions, predicts

$$S_A = \frac{1}{2}\int_0^1 \frac{dx}{x}\{F_2^{\nu n} - F_2^{\nu p}\} = (U - \overline{U}) - (D - \overline{D}) = 1$$

since the net number of $u$-type less $d$-type quarks in the proton is unity. Thus far, there is only one measurement of this quantity in the literature [10], which gives $S_A = 1.01 \pm .20$.

- Gottfried Sum Rule [11], obtained from charged lepton scattering measurements

$$S_G = \int_0^1 \frac{dx}{x}\{F_2^{\mu p} - F_2^{\mu n}\} = [e_u^2 - e_d^2][(U + \overline{U}) - (D + \overline{D})] = \frac{1}{3} \qquad (5)$$

The experimental determination disagrees with this prediction. We will return to this question.

| Date | Expt | Value |
|---|---|---|
| $< 1990$ | EMC | $0.24 \pm 0.11$ |
| 1991 | NMC | $0.24 \pm .016$ |
| 1993 | NMC | $0.258 \pm 0.017$ |

Table 1: *Gottfried Sum Rule Experimental Values*

- Gross-Llewelyn Smith Sum Rule [12], calculated from the valence quark distribution

$$S_{GLS} \equiv \int_0^1 \frac{dx}{x} x F_3^{\nu N} = (U - \overline{U}) + (D - \overline{D}) = 3 \qquad (6)$$

is equal to the total number of valence quarks in the nucleon. We shall see that this naive prediction is also not experimentally satisfied, though the QCD corrections, now calculated up to third order, bring the predictions into close agreement.

- Bjorken Sum Rule [13], obtained from the neutron and proton spin structure functions,

$$S_{Bj} \equiv \int_0^1 \frac{dx}{x}\{g_1^n - g_1^p\} = \frac{1}{2}[e_u^2 - e_d^2]\underbrace{[(U^\uparrow - U^\downarrow) - (D^\uparrow - D^\downarrow)]} = \frac{1}{6}\left[\frac{g_A}{g_V}\right] \qquad (7)$$

is predicted in terms of the net numbers of aligned up and down quarks. The quantity in brackets is the expectation value of the axial current times third component of isospin, or the axial coupling. Again, the measurements of this are precise enough that at lower $Q^2$, the QCD corrections are important.

## 2.1 Gottfried Sum Rule

This sum rule has not agreed with experiment for several years. Table 1 shows that the experimental value is lower than the prediction $S_G = 0.33$ in equation (5). The entries show results from earlier analyses [14], as well as a more recent re-evaluation [15] using NMC data alone. Figure 1 shows



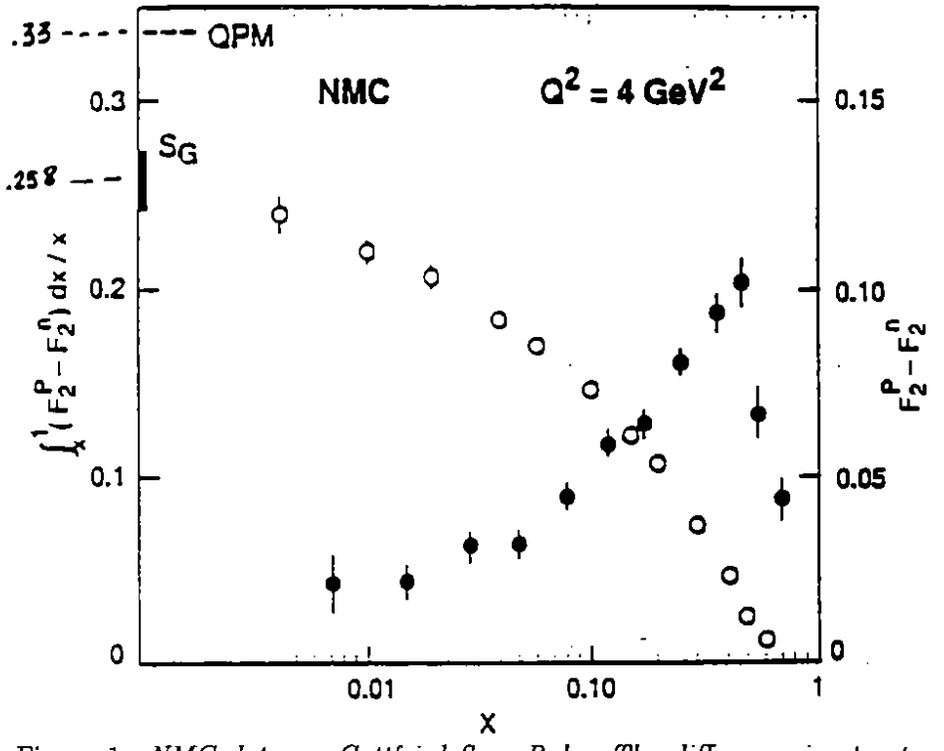


Figure 1: *NMC data on Gottfried Sum Rule. The difference in structure functions is shown as filled points with the right-hand scale and the integral is shown as open points with the left-hand scale.*

the measurements relevant to these data, which clearly disagree with the prediction.

There are many possible explanations postulated for this deficit, including [16] an anomalous $x$-dependence for the difference between the proton and neutron structure functions in the unmeasured region $x < .004$, uncorrected shadowing effects, and possible QCD corrections. Some or all of these may be relevant, but it is highly likely that the difference between the $\overline{d}$-quark and the $\overline{u}$-quark distributions plays a substantial role [17].

The Gottfried sum rule prediction of precisely $1/3$ does not, in fact, follow from current algebra. Indeed, even within the quark model it is not rigorous. Equation (5) may be expressed, after imposing a net total of two $u$-quarks

and one $d$-quark in the proton, as follows:

$$S_G = \frac{1}{3} - \frac{2}{3}\left[\overline{D} - \overline{U}\right].$$

This implies that $S_G = 0.33$ only if the net number of sea $\overline{d}$-quarks equals the number of sea $\overline{u}$-quarks. There is no fundamental principle that requires this, and there may even be good reasons to expect that it *not* happen. Indeed, this was recognized in one of the earliest discussions of the quark flavor distributions [18]. We will discuss this issue more fully in the section dealing with quark densities.

## 2.2 Gross-Llewelyn Smith (GLS) Sum Rule

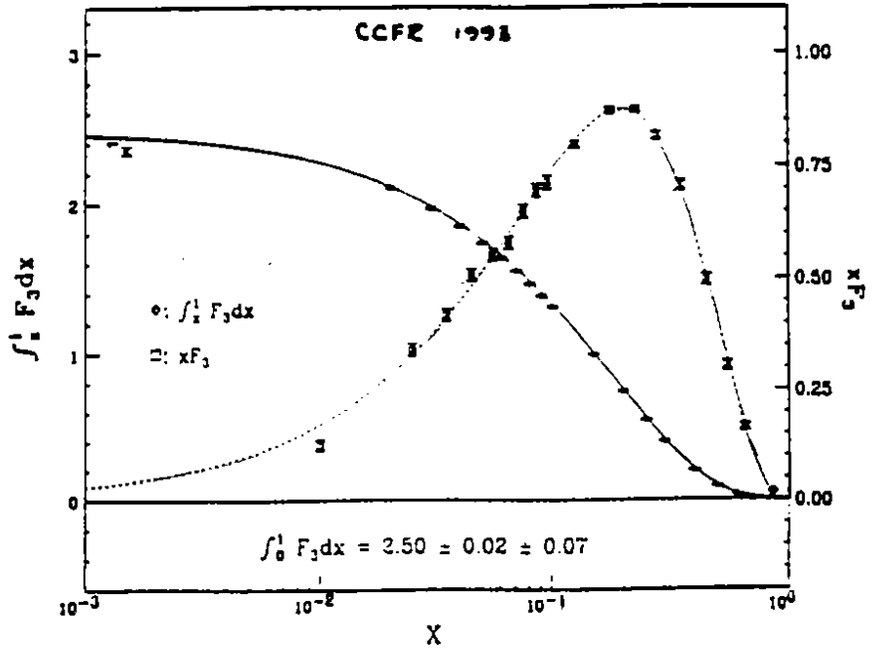


Figure 2: *CCFR data on the Gross Llewelyn-Smith Sum Rule. The differential $xF_3$ function corresponds to the right-hand scale and the monotonic integral to the left-hand scale.*



The most recent measurement [19] of $xF_3$ is shown in figure 2 at momentum-transfer, $Q^2 = 3\ GeV^2$. The best experimental value for the integral, extrapolated to $x = 0$ is

$$S_{GLS}^{CCFR} = 2.50 \pm .02 \pm .07$$

which is more than seven standard deviations from the naive QPM prediction of 3.0 given in equation (6)!

This brings us to an important point: the sum rules typically have sizable QCD corrections dependent on the quark-gluon coupling, $\alpha_s(Q^2)$. Recently these have been calculated [20] up to order $\alpha_s^3$ for both the GLS and the Bjorken sum rules. In general, they have the form

$$S(Q^2) = S_0\left[1 - \left(\frac{\alpha_s}{\pi}\right) - C_1\left(\frac{\alpha_s}{\pi}\right)^2 - C_2\left(\frac{\alpha_s}{\pi}\right)^3\right]$$

where, for example in the GLS case, $C_1 = 3.25$ and $C_2 = 12.2$ . This modifies the prediction for the GLS sum rule so that at $Q^2 = 3\ GeV^2$, where we take $\alpha_s = .30 \pm .03$, the expected result is

$$S_{GLS}^{pred} = 2.59 \pm .06$$

which is in good agreement with the experimental result shown in figure 2. It is interesting to note that a 10% error on $\alpha_s(3\ GeV^2)$ creates predictive uncertainty comparable to that of the experiment.

## 2.3 Bjorken Sum Rule

This relation (7) was originally thought to be "worthless" by its creator [21], mainly because the idea (in 1966) of measuring cross-sections over a large part of the kinematic regime for scattering of polarized leptons from polarized protons and neutrons did not seem realistic. Well, it is now being done with some precision. Historically, our interest became piqued by a measure [22] of $g_1^p$, the proton spin structure function, in 1987 by EMC which, combined with an earlier SLAC measure, gave a surprising result (which we discuss and update later). The feasibility of testing the sum rule became apparent; and last year results were presented on $g_1^n$ from two groups [23]. These are summarized in table 2, together with predictions with $\alpha_s^3$ QCD corrections.

| Group | $Q^2$ | $S^{pred}$ | $S^{meas}$ |
|---|---|---|---|
| SMC | 5 $GeV^2$ | $0.191 \pm .002$ | $.20 \pm .06$ |
| E142 | 2 $GeV^2$ | $0.184 \pm .007$ | $0.146 \pm .021$ |
| Combined | 5 $GeV^2$ | $0.185 \pm .004$ | $0.181 \pm .032$ |

Table 2: *Measurements of Bjorken Sum Rule*

The conclusions from the two groups appear to be at odds, with the SMC (CERN) value agreeing with prediction and the E142 (SLAC) value disagreeing. But figure 3 shows the comparison of $xg_1^n(x)$ as measured directly from $He^3$ by SMC and as inferred from the deuteron measurements by the E142 group. Though the error bars are larger, the SMC data extend to smaller values of $x$. The extrapolation at low $x$, as indicated in the figure, is very sensitive to the small $x$ behavior and the $1/x$ in the integrand for the sum rules is sensitive to the extrapolation. The bottom entry in table 2 gives the

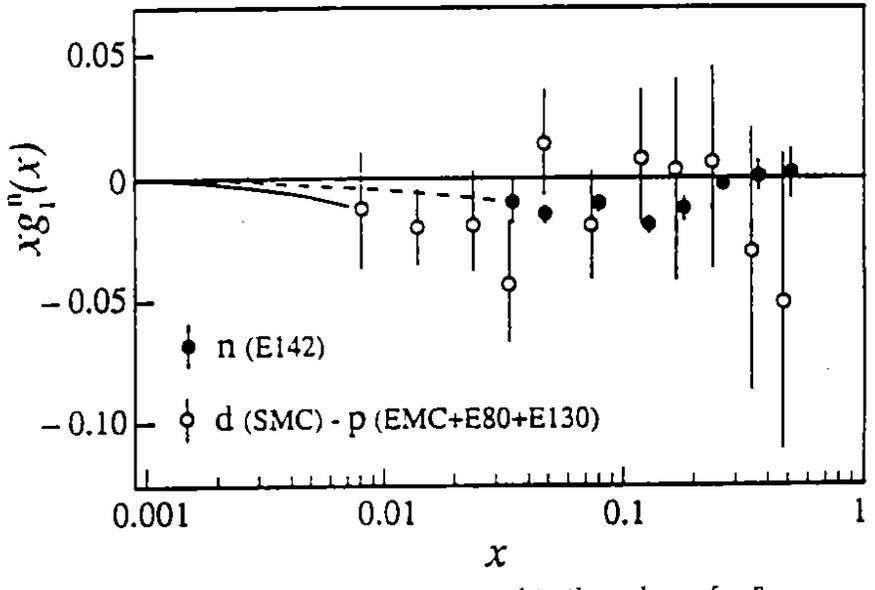


Figure 3: *The closed data points correspond to the values of $xg_1^n$ measured by E142 and the open data points to the values calculated from the measurements of deuterium by the SMC group. The latter have larger errors but extend to smaller values of $x$.*



value using both sets of data; it is in good agreement with the prediction. We will discuss quark spin density issues more later.

# 3 Quark Densities

The information from the fixed target experiments permit us to measure the densities of the various flavors of quarks inside the nucleon. We proceed to describe these and how they are obtained.

## 3.1 Valence and Sea

Structure function measurements using isoscalar targets (with equal numbers of neutrons and protons) directly specify the valence (see figure 2) and sea distributions. As stated previously, the measurement of $xF_3$ in neutrino-nucleon interactions determines the valence, or $x(u+d-\overline{u}-\overline{d})$, distribution. Up to corrections from the $s$- (or strange) quarks, the $F_2$ measurement (from either neutrino or electron/muon scattering) determines the $x(u+d+\overline{u}+\overline{d})$ spectrum. The sums and differences of these two gives a direct measure of

$$q(x) = u(x) + d(x)$$
$$\overline{q}(x) = \overline{u}(x) + \overline{d}(x)$$

These distributions are shown in figure 4 as derived from measurements by the CCFR group [5] at $Q^2 = 25\ GeV^2$. The antiquark ($\overline{q}$) distribution is half the total quark-antiquark sea. The dependence of $q(x)$ and $\overline{q}(x)$ at very large $x$ are constrained by complementary measurements of the Drell-Yan processes [25], $p + p \rightarrow \mu^+ + \mu^- + X$.

Measurements of $F_2^{\mu N}$ from precision muon-nucleon scattering over the same energy region are consistent with the $F_2^{\nu N}$ used here and the mean-square charge hypothesis described earlier, with some reservation expressed for the small $x$ region (which we discuss later in conjunction with the nucleon strangeness content). These high precision isoscalar measurements form the basis of our knowledge of quark densities.

## 3.2 Separation of $u$ and $d$ ($\overline{u}$ and $\overline{d}$)

It is possible, in principle, to measure each of the flavor distributions by exploiting the $y$-dependence [4] of $\nu$ and $\overline{\nu}$ scattering from hydrogen and

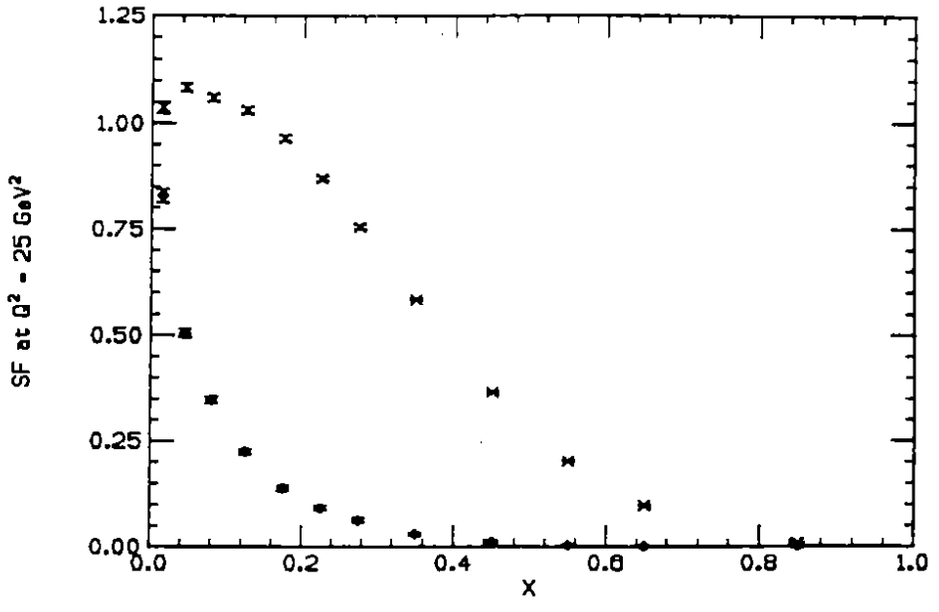


Figure 4: *The quark (upper curve shown as x's) and antiquark (low curve shown as diamonds) distributions with statistical errors shown for* $Q^2 = 25\ GeV^2$. *The data correspond to* $x$ *times the probability for finding a quark (antiquark) between* $x$ *and* $x + dx$.

deuterium targets. In practice, this technique does not work well: large statistical and systematic errors result when this has been tried [24]. Charged lepton scattering from hydrogen and deuterium targets is more precise, but can only separate according to electric charge. The ratio of these structure functions is given by

$$\frac{F_2^{en}}{F_2^{ep}} = \frac{1 + 4\frac{d+\bar{d}}{u+\bar{u}}}{4 + \frac{d+\bar{d}}{u+\bar{u}}}$$

to provide a direct measure of the $\frac{d+\bar{d}}{u+\bar{u}}$ ratio; the recent, precise measure [15] analogous to earlier data of figure 1 continues to indicate that $d(x)$ falls faster than $u(x)$ by about a factor of $(1 - x)$.

A very interesting presentation at this conference was the measure of the charge asymmetry of final state leptons from $W^{\pm}$ production by CDF at the Tevatron collider [26]. The technique relies on the fact that the dominant



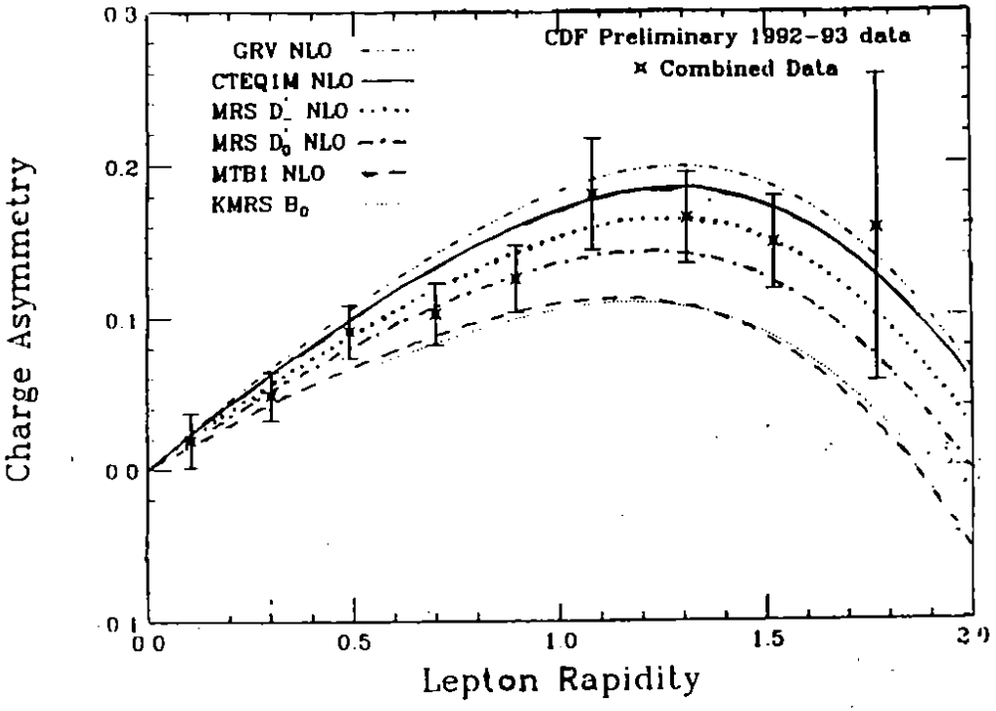


Figure 5: *The data on the charge asymmetry of the decay lepton from W-decay versus the lepton psuedorapidity from the CDF collider group. Curves from different parameterizations of the* $u/d$ *ratio are also shown. See text.*

production mechanism for positively charged vector bosons comes from annihilation of $u$-quarks in the proton by $\overline{d}$-quarks in the antiproton, and the reverse for negatively charged bosons. The differential cross-section per unit of $W$ rapidity, $\eta_W$, may be expressed

$$\frac{d\sigma}{d\eta_W}\left(p + \overline{p} \rightarrow \begin{matrix} W^+ \\ W^- \end{matrix} + X\right) = Cx\overline{x}\begin{pmatrix} u(x)\ d(\overline{x}) \\ d(x)\ u(\overline{x}) \end{pmatrix}$$

where $x(\overline{x})$ is the fraction of the colliding quark in the $p(\overline{p})$, respectively. Here

$$\eta_W = \log\left[\frac{M_W}{\sqrt{s}}x\right] = -\log\left[\frac{M_W}{\sqrt{s}}\overline{x}\right]$$

Since the $u$-quark density is typically larger than the $d$-quark density in the proton, we expect more $W^+$ in the positive rapidity region and more

$W^-$ at negative rapidity. The expected asymmetry versus $\eta_W$ monotonically increases, but only the charged lepton from the decay $W^\pm \to l^\pm + \nu_l(\overline{\nu}_l)$ is actually observed. The V-A decay causes the asymmetry at very large values of the lepton rapidity, $\eta_l$, to fall to zero. The observed asymmetry reflected about $\eta_l = 0$, shown in figure 5, is sensitive to the $\frac{d(x)}{u(x)}$ ratio in the region $0.01 < x < 0.3$. Superimposed on the measured data are curves calculated from various structure function parameterizations. These preliminary data already verify that the $d/u$ ratio measured at small space-like $Q^2$ is similar to that measured at time-like $Q^2 = -M_W^2$ , and they promise a precise measure of quark flavor ratios in the future.

Unfortunately, neither technique separates quarks from antiquarks. Until recently, when the Gottfried sum rule was found to be unsatisfied (described in section 2), the seas were assumed equal[3] : $\overline{d} = \overline{u}$. A suggestion [27] has been followed to use the Drell-Yan process involving the asymmetry of lepton pairs for $pp$ and $pn$ scattering by two experiments: NA51 at CERN and E886 at Fermilab. Thus far, only a single point is available (from NA51), which indicates [28] an asymmetry of the *opposite* sign than one might naively expect at $x \approx 0.2$ either for $\overline{u} = \overline{d}$ or for the small difference required to satisfy the Gottfried sum rule. A functional form for $\overline{u} - \overline{d}$ exists [29] which agrees with this point and with the Gottfried prediction, but it is not a simple monotonic function. There is more to be understood about the difference $\overline{u} - \overline{d}$, but this will require a very complete analysis of all the elements contributing to the Gottfried sum rule as well as very good Drell-Yan measurements.

## 3.3 Strange (and higher mass) Sea Constituency

The most direct method for measuring the intrinsic constituency of the strange sea in the proton comes from measurements of dimuon processes in neutrino collisions. The relevant elementary reactions are

$$\begin{aligned} \nu_\mu + (d, s) &\to \mu^- + c + X \\ c &\to \mu^+ + X' \end{aligned} \qquad (8)$$

for charm quark production and decay. This mechanism results in two opposite-sign muons; the process initiated by antineutrinos occurs from $(\overline{d}, \overline{s})$

[3] An important historical exception may be found in the classic work by Field and Feynman [18].



quarks and also results in two oppositely charged muons. The relatively small numbers of same sign dimuons demonstrates that reactions (8) represent the dominant mechanisms for production of dimuons.

Quantitative analyses of $\mu^+\mu^-$ neutrino data permit measures of the relevant Cabibbo-Kobiyashi-Moskawa matrix elements and of the strange sea. Traditionally, the latter has been described by the parameter

$$\kappa(x) = \frac{2s(x)}{\overline{u}(x) + \overline{d}(x)}$$

which is defined such that $\kappa = 1$ indicates an "$SU(3)$ symmetric sea". Experimentally, experiments have typically obtained $\kappa \approx 0.5$. A recent high-statistics measurement, utilizing next-to-leading order treatment[30] of the final-state massive quarks systems, gives[31]

$$\kappa = 0.435 \pm 0.059$$

for the strange sea fraction.

There is also indirect sensitivity to the strange sea fraction from deviations from the 5/18 rule at small $x$ due to the strange/charm asymmetry:

$$\frac{F_2^{\mu N}}{F_2^{\nu N}} = \frac{5}{18}\left[1 - \frac{3}{5}\frac{s + \overline{s}}{q + \overline{q}}\right]$$

The correction term inside the brackets is small. One version of structure function parameterizations (CTEQ1) exploited a small additional difference between NMC muon data and CCFR neutrino data (about 3% at $x = .08$) at small $x$ to quote a substantially larger strange sea than warranted by the dimuon data. Such differences between these data sets are near the level of normalization errors quoted by the experiments and thus do not constitute strong evidence to contradict results from more direct methods.

If there are subtle mechanisms [32] involving massive quarks beyond those calculable from straightforward QCD techniques [30], experimenters should re-visit their error analysis at small $x$ before firm conclusions are drawn. It should be noted that, besides strange sea effects involving charm thresholds, there are other important differences expected between neutrino and charged lepton structure functions at small $x$. It has been noted [33][34], for example, that the values of $F_2^{\mu N}$ and $F_2^{\nu N}$ as $Q^2 \to 0$ must be different, even with only

$u$-quark and $d$-quark contributions, because of the presence of the axial vector current in the charged current process.

Measurements [35] of associated charm production in muon nucleon scattering has permitted extraction of the charm sea component of the nucleon. As expected, this component is very small [34] in the fixed target regime. Densities of higher mass $b$-quarks are undoubtedly even smaller, a topic that HERA might address.

### 3.4 Quark Spin Densities

Measurements of the spin structure functions, $g_1^p$ and $g_1^n$, permit estimation of the spin content of the nucleon [36]. The following relations follow from the naive parton model, where the net spin carried by $u$-type quarks in the proton is given by $\Delta U = U^{\uparrow} - U^{\downarrow} + \overline{U}^{\uparrow} - \overline{U}^{\downarrow}$, *etc* as described in equation (7)

$$\Gamma_1^p = \int g_1^p(x)\ dx = \frac{4}{18}\Delta U + \frac{1}{18}\Delta D + \frac{1}{18}\Delta S$$

$$\Gamma_1^n = \int g_1^n(x)\ dx = \frac{1}{18}\Delta U + \frac{4}{18}\Delta D + \frac{1}{18}\Delta S$$

where the latter relation follows from isospin symmetry. Hence, measurements of both integrals, besides providing a test of the Bjorken sum rule, give two relations among the contributions to the proton spin of the three quark types. If one further assumes flavor $SU(3)$ symmetry, an additional relationship may be found in terms of the two constants, $F$ and $D$, representing two irreducible matrix elements of the axial currents obtained from $g_A$ and hyperon beta decay. This assumption permits extraction of the individual spin contributions to the proton by the three types of quarks, whose sum $\Sigma = \Delta U + \Delta D + \Delta S$, gives the net quark contribution to the proton spin. If one makes the further assumption that $\Delta S = 0$, the Ellis-Jaffe sum rule [37] follows, which predicts the values of $\Gamma_1^n$ and $\Gamma_1^p$ in terms of the $F$ and $D$ constants.

When the proton structure function was measured [22] several years ago, it appeared that the data were inconsistent with the Ellis-Jaffe sum rule, and that the total contribution of quarks to the proton spin was small ($\Sigma = 0.12 \pm 0.17$). This observation has been dubbed the "spin crisis". As already discussed, last year saw measurements [23] of the neutron spin structure function by two groups.



| Measure | $\Sigma$ | $\Delta s$ |
|---|---|---|
| Proton average | $0.30 \pm 0.13$ | $-0.09 \pm 0.04$ |
| Neutron average | $0.24 \pm 0.23$ | $-0.11 \pm 0.08$ |
| Overall average | $0.28 \pm 0.11$ | $-0.09 \pm 0.04$ |

Table 3: *Net quark contribution to spin ($\Sigma$) and strange quark contribution ($\Delta s$) from average of proton, neutron, and all data.*

At this conference, we have seen a presentation of new measurements [8] of the proton spin structure function to much smaller values of $x$ than previously measured. A fit by the SMC group to the world's data on $g_1^p$ gives a measurement, $\Gamma_1^p = 0.145 \pm 0.01 \pm 0.012$, to be compared with the Ellis-Jaffe sum rule prediction of $0.177 \pm 0.003$. While these are still different, the discrepancy has narrowed to about two standard deviations. Furthermore, the calculated values $\Sigma$ versus $\Delta S$ from the various measurements bracket a broad range, but there is general agreement that there is a net positive contribution from quarks, while from strange quarks the contribution is slightly negative. Table 3 summarizes these conclusions by the SMC group. Similar conclusions have been drawn by others [36].

## 4 R, QCD, Gluons, and GLAP Evolution

The above discussions indicate that the quark densities are generally well measured and well understood in the "fixed target" kinematic region

$$.01 < x < 1$$
$$2 < Q^2 < 400\ GeV^2$$

obtained, for the most part, from a body of fixed target lepton-nucleon programs carried out over the past two decades. These experiments have been a diverse group using electron, muon, and neutrino beams under many different conditions of energy, target, and polarization which ultimately provided samples approaching millions of events each. There are still some loose ends that require further attention, but the foundation is firm. It is exciting to see that information is corroborated and supplemented by Drell-Yan experiments for the $\overline{u}/\overline{d}$ ratio and by collider data on $W^{\pm}$ production to extract $u/d$.

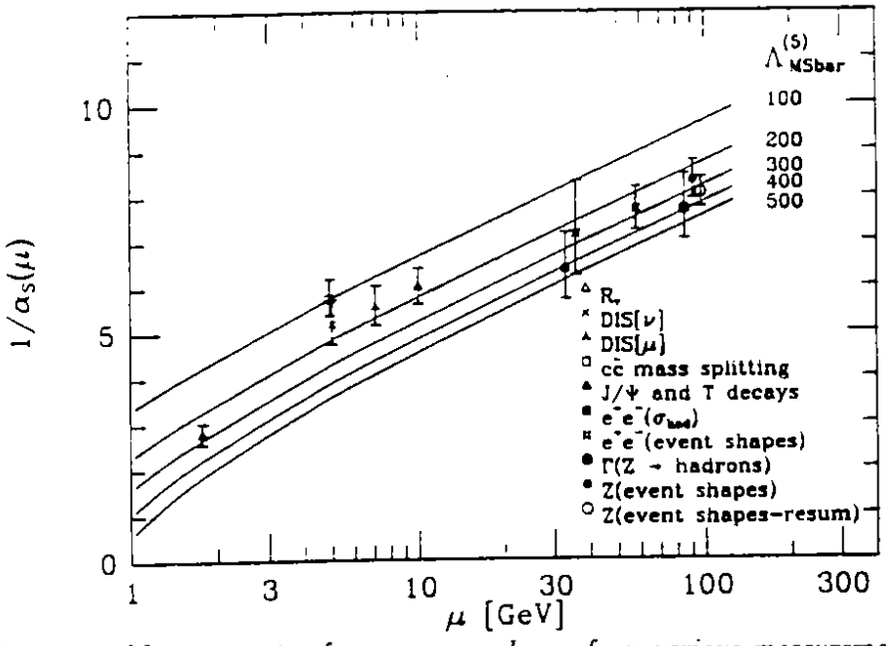


Figure 6: *Measurements of $\alpha_s$ versus scale, $\mu$, from various measurements as shown. See text.*

The current algebra sum rules are in *excellent* shape after correction for known perturbative QCD effects up to order $\alpha_s^3$. There are still questions about the effects of even higher order and of higher twist corrections, but these will only be answered by calculation or by measurement of nonsinglet structure functions at even higher $Q^2$.

Even the elusive $R = \sigma_l/\sigma_t$ seems to be reasonably well known in this kinematic regime[26]. Though the rather poor measurements at larger $Q^2$ are consistent with the requirements of QCD and target mass effects, additional higher twist corrections are required in the lower $Q^2$ range.

Tests of perturbative QCD in deep inelastic scattering are *independent* of $R$ or of the gluon density, $g(x, Q^2)$, when using nonsinglet or valence-type structure functions. Such tests, both for neutrinos [38] and muons [39] indicate good consistency with the evolution equations. Global fits to singlet data [38][39], fitted to parameterized gluon distributions, give measurements of the quark-gluon coupling consistent with the nonsinglet fits. Even more impressive, many *different* methods of extracting this coupling give very consistent results. This is illustrated [40] in figure 6, which shows $1/\alpha_s(\mu)$ versus the scale, $\mu$, as measured in a multitude of processes. The curves correspond to various assumptions for the scale parameter, $\Lambda^{(5)}_{\overline{MS}}$. The agreement with the $\Lambda^{(5)}_{\overline{MS}} = 200\ MeV$ curve is impressive.



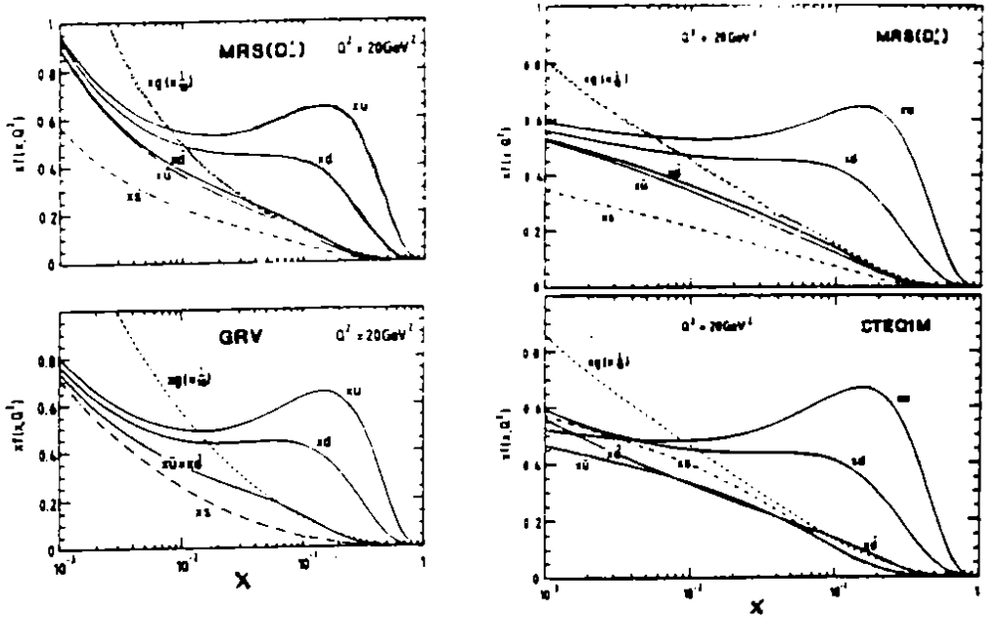


Figure 7: *The gluon and quark distributions of assorted flavors according to the parameterizations of the MRS, CTEQ, and GRV groups. The $MRS(D_-)$ and $MRS(D_0)$ differ in that the former assume gluon and sea distributions which fall like $x^{-1/2}$, while the latter assume these flat ($\sim x^0$, at small $x$).*

We are fortunate to have several dedicated phenomenology groups who collect all of the relevant information and provide us with GLAP evolutions of all the flavor distributions, including gluons. Examples of these densities [41][42][43] are shown in figure 7. It should be noted that the quark densities in the fixed target regime generally agree well[4].Even the gluon densities provided by the various parameterizations in the fixed target regime agree at

[4]The single exception are the CTEQ1 parameterizations for the $s$-quark density, which are larger because of the interpretation of small $x$ differences cited above. This has been corrected in CTEQ2 densities.

the 20% level, which might be taken as an indication of how well $g(x, Q^2)$ is known there. The gluon density is constrained [44] primarily by the momentum sum rule and measurements of single photon production in $pp$ collisions [45], from the elementary process $gq \rightarrow \gamma q$ at large $x$, in addition to the requirements of GLAP structure function evolution.

But once we go to values of $x$ below those accessible by fixed target experiments, the situation is very different. In figure 7, there are differences of more than a factor of two in both quark and gluon densities for $x \approx 10^{-3}$ among the several phenomenological fits, and the divergence grows at smaller $x$. This is, of course, because the GLAP evolution only relates the $Q^2$-dependence at a specific value of $x = x'$ to integrals over structure functions for all $x > x'$; it follows, therefore, that GLAP tells us little directly about the behavior of structure functions below the $x$-region we have already measured (or hypothesized). At best, we can only tell whether, after they are measured, they are *consistent* with traditional perturbative QCD evolution. And given the broad freedom in parameterizing sea and gluon inputs to these fits, it is *unlikely* that we will *not* make good fits[5]. The advent of HERA data gives us the experimental input we need to put into these parameterizations, but is this enough? We will return to this question later. Now let us turn to the new kinematic regime of HERA.

# 5 The New Regimes of HERA

The electron-proton collider, HERA, has now been in operation for nearly two years. During this period the electron energy ($E_e$) has been 26.7 $GeV$ and the proton energy ($E_p$) 820 $GeV$. These values provide center-of-mass energy close to the design value (300 $GeV$). From the beginning, it has been clear that electron polarization capabilities are there; transverse polarizations of about 70% have been measured[46] and high longitudinal polarization will be available for physics in the longer term.

[5]It should be noted that the approach of the GRV group is to fit all structure function data in the fixed target regime using only parameterizations of the "valence-like" distributions of the valence, sea, and gluon components at $Q^2 = 0.25\ GeV^2$. In contrast with the MRS and CTEQ approaches in which the small $x$ parameterizations of the sea and gluons are arbitrary, the GRV ansatz provides a prediction for the small $x$ regime of HERA (up to the freedom permitted in parameterizing the valence-like distributions at larger $x$ and low $Q^2$).



| Run Dates | $\int \mathcal{L} dt$ | NC events | CC events | Analysis |
|---|---|---|---|---|
| Jun-Aug 1992 | $2\ nb^{-1}$ | 300 | 0.1 | Complete |
| Oct-Nov 1992 | $30\ nb^{-1}$ | 5000 | 1 | Complete |
| Jun-Oct 1993 | $0.5\ pb^{-1}$ | $10^5$ | 25 | In Progress |
| 1994 | $5\ pb^{-1}$ | $10^6$ | 300 | Hope |
| Design/year | $100\ pb^{-1}$ | $10^7$ | 5000 | Long Term |

Table 4: *History and projections of HERA luminosity.*

The data compared here are from the 1992 running period, from which structure functions have been published [47][48]. New data, from the 1993 running period, are included in the plenary session [49][50]. There also exists a considerable body of information on non-standard model searches [51] and photoproduction [52] , which are not highlighted at this structure function workshop.

The luminosity at HERA started low but has been systematically rising, as seen in table 4. Though the data rates began lower than the design value, increases thus far have been impressive, with about 0.5 $pb^{-1}$ presently being analyzed by each group and as much as an order of magnitude increase expected for the next year.

For measurements of structure functions, there are two DIS processes of interest at HERA. First, the charged current (CC) reaction, $e^- + p \rightarrow \nu_e + X$ , is directly analogous to the neutrino-initiated process described earlier. Table 4 shows that the rate for this reaction is not yet high enough to be useful for even crude measurements of structure functions. The important reaction at present luminosities is the neutral current (NC) process, $e^- + p \rightarrow e^- + X$, in which the exchange of a virtual $\gamma$ is dominant.

HERA covers two entirely new kinematic regimes:

- High $Q^2$ : At $Q^2 \geq 1000\ GeV^2$, one can observe effects of the $Z^0$-exchange as well as find unexpected structure or new phenomena of many types. Limits have already been placed[51] on many phenomena outside the Standard Model. However, the unique sensitivities inherent

in an $ep$ collider will require high luminosities.

- Very low $x$ at moderate $Q^2$ : The region with $10^{-5} < x < 10^{-2}$ is not yet explored. Techniques for extrapolation in $Q^2$ using the GLAP perturbative expansions in the quark-gluon coupling constant, $\alpha_s$, have been successful with fixed target experiments. By itself, GLAP conveys little information on the $x$-dependence and, in any case, the expansion is bound to break down at very small $x$ when parton densities become very large.

# 6 Detectors at HERA

H1 and ZEUS are state-of-the-art collider detectors that are well documented elsewhere[53][54]. It should be recalled that, for electron-proton collisions, the detectors are unlike those to which people are probably accustomed: they are asymmetric, with more calorimeter mass and tracking volume in the direction of the more energetic proton beam. The groups have adopted a coordinate system with the proton beam direction taken as the positive $z$-axis and polar angle $\theta = 0°$.

In brief, the ZEUS detector contains an hermetic Uranium-scintillator calorimeter that has operated reliably from the beginning. For the early data described here, the forward and rear tracking had not yet been completed and only three superlayers of the central tracking readout was operational.

H1 has had complete tracking from the beginning, and it has operated well. The calorimeter contains liquid Argon as the active medium except within about 20° from the direction of the electron beam, where a plug electromagnetic calorimeter is incorporated with warm scintillator as the active medium and a tracking plane is located just upstream.

Both detectors utilize *luminosity* monitors (LUMI) in the electron direction. These consist of detectors for recording the final state electron and photon from the bremsstrahlung process $e^- + p \rightarrow e^- + \gamma + p$. The well understood cross-section of this process is the basis for measurements of the luminosity ($\mathcal{L}$). The electron components of the luminosity monitors also record electrons for analysis of photoproduction processes, largely inelastic reactions involving almost real photons ($Q^2_{\max} \approx .03\ GeV^2$).



# 7 Triggering and Selections

The topologies for DIS processes are highly distinctive. For the NC process, an electron which is typically well-isolated from other particles is visible in the detector. The triggering to isolate NC interactions is designed mainly to rid the sample of background due to interactions of the proton beam with residual gas in the beam vacuum pipe. There are many handles to remove this background, from the obvious requirement for a vertex inside the known interaction region to the more subtle requirement that the timing of the calorimeter energy depositions be consistent with particles emanating from the interaction region.

An isolated electron above some minimum energy identified within the fiducial volume further refines the sample of DIS events. At this juncture, the background consists primarily of photoproduction events in which the final state electron has continued down the beam pipe (but missed the electron detector in the LUMI), and in which misidentification of an electron has resulted from the central detector information. This background can be reduced further by applying the "$E - p_z$" constraint.

It is a truism that lepton-nucleon experiments at present colliders lie intermediate in available center-of-mass energy between hadron and electron collider experiments. But this middle ground also applies to the relative *cleanliness* for isolating specific final states, exemplified by the number of usable constraints. In typical $e^-e^+$ scattering events, conservation of energy-momentum provides four constraints; in $\overline{p}p$ events, only conservation of the two transverse momentum components is useful. In $e^-p$ neutral current collisions, there are *three* useful constraints.

Besides transverse momentum, one additional conservation rule is useful:

$$E - p_z = 2E_e \tag{9}$$

where $E_e$ is the initial electron beam energy, and $E(p_z)$ is the energy (beam component of momentum) summed over all final state particles. This particular combination is *insensitive* to the proton beam remnant which exits through the beam pipe in the proton direction. It is *extremely* sensitive, on the other hand, to whether an electron has been missed by the detector in the electron beam direction, which is precisely what happens in photoproduction background events.

The distribution in the reconstructed value of $E - p_z$ for DIS events peaks near 52.3 $GeV$, with a small low energy radiative tail. In general, relation (9) will *not* be satisfied by photoproduction processes: a somewhat smaller value will be measured. Requiring an identified final state electron reduces the photoproduction background by more than two orders-of-magnitude, but still leaves photoproduction events with a *misidentified* electron candidate as the dominant background to DIS. Requiring a minimum value for $E - p_z$ removes most of that remaining; additional cuts can lower it even further. In detail, the magnitudes of such backgrounds differ in each kinematic region.

## 7.1 Kinematic Parameters

### 7.1.1 Calculations of Variables

Because in NC events the final state electron and hadron energies are over-constrained, there are choices [55] for how the kinematic parameters $Q^2$, $x$, and $y$ will be determined. At our disposal are the energy and angle of the electron ($E'_e$ and $\theta$ , respectively), as well as the vector sums of the hadronic energy in the transverse and longitudinal directions ($p_x$ , $p_y$ , and $p_z$ , respectively).

The parameters obtained from the electron energy ($E'_e$) and angle ($\theta$) are given by

$$Q^2_e = 4E_e E'_e \cos^2\frac{\theta}{2} \tag{10}$$

$$y_e = 1 - \frac{E'_e}{E_e}\sin^2\frac{\theta}{2} \tag{11}$$

$$x_e = \frac{Q^2_e}{sy_e} \tag{12}$$

where $\theta$ is measured with respect to the direction of the proton beam.

Alternatively, the $y$-variable can be determined from

$$y_h = y_{JB} = \frac{1}{2E_e}\sum_h (E - p_z) \tag{13}$$

where the sum is over all final state hadrons[6].This *hadronic* measurement

[6]In practice, the energy deposits measured in the calorimeter are used for measuring the sum in equation (9). The sum in (13) is done similarly, with the exclusion of the electron.



is sometimes called the "Jacquet-Blondel" measurement of $y$. The measurement of $x$ may also be obtained by utilizing the latter $y$-estimate

$$x_m = \frac{Q^2_e}{sy_h} \tag{14}$$

said to be obtained from "mixed variables".

In addition we may define an "effective angle", $\gamma$, for the direction of the scattered hadronic system

$$\cos\gamma = \frac{(\sum p_x)^2 + (\sum p_y)^2 - (\sum(E - p_z))^2}{(\sum p_x)^2 + (\sum p_y)^2 + (\sum(E - p_z))^2}$$

where the sums extend over all final state hadrons. Note that the estimates of both $y_h$ and $\gamma$ are insensitive to unobserved final state energy in the direction of the proton beam. The angles of the electron and the scattered hadronic system provide

$$Q^2_{DA} = 4E^2_e \frac{\sin\gamma\,(1 + \cos\theta)}{\sin\gamma + \sin\theta - \sin(\theta + \gamma)}$$

$$x_{DA} = \frac{E_e}{E_p}\frac{\sin\gamma + \sin\theta + \sin(\theta + \gamma)}{\sin\gamma + \sin\theta - \sin(\theta + \gamma)} \tag{15}$$

These "double angle" estimates of the kinematic variables have the virtue that they are relatively insensitive to the absolute energy scales for measurement of final state electrons and hadrons.

It should be noted that the equivalence of *all* these estimates are consequences *only* of energy-momentum conservation, and do not *in fact or principle* require finding a final state hadronic jet.

### 7.1.2 Reflections on Variable Choices by H1 and ZEUS

The H1 group select only electrons entering their plug electromagnetic calorimeter; these are calibrated by comparing against Monte Carlo expectations to provide estimates of their energy scale uncertainty to be about 2%. They utilize the ($Q^2_e$, $x_e$) estimates over most of the kinematic regime and ($Q^2_e$, $x_m$) over the remainder.

ZEUS uses electrons over the entire solid angle of the calorimeter. The data exhibit systematic shifts in electron energy scale relative to that ex-

pected from test beam measurements.[7] To minimize reliance on the reconstructed energy scale, they have opted to use the estimators $(Q^2_{DA}, x_{DA})$ which has the virtue that the energy scale for the event variables comes directly from the beam energies.

The estimates of the $y$-variable described in equations (11) and (13) carry important implications for both backgrounds and resolutions. Note that $y_e = y_h$ is formally equivalent to the constraint equation (9), so an equivalent signature for photoproduction background is $y_e > y_h$. Photoproduction events that *do* survive cuts on $E - p_z$ contain falsely identified electrons. This is much more likely for *low energy* electrons, since smaller depositions of energy provide calorimeter patterns that are less unique than those of high energy. Furthermore, in photoproduction events, isolated energy deposits with low energy are more likely to occur than those with higher energy. As consequence, background events tend to have *small* values of $E'_e$ and, from equation (11), *large* values of $y_e$. The experimental groups place cuts on *both* small $E - p_z$ and large $y_e$ to remove photoproduction background.

Good resolution is essential for the $x$-variable. But all methods of estimating $x$ require a correspondingly good measure of $y$, as can be seen directly in equations (12) and (14). But the fractional error in y *always* becomes poor at small $y$.[8]The resolution at small $y$ from equation (11) is $\Delta y_e \approx \frac{\Delta E_e}{E_e} \geq .05$ , for relevant electron energies. Similarly, the hadronic measure $(y_h)$, though directly proportional to total hadronic energy, is limited to similar values at low energy by issues like detector readout noise and zero suppression techniques.

The ZEUS group has opted to make a fixed cut on $y_h$, and H1 has chosen to place all events with $y_e$ below a certain value into a single bin which is then divided among the $x$-bins from Monte Carlo calculations based on fixed target muon data.

## 7.2 Experimental Selections

[7]This effect has recently been understood in terms of the detailed distribution of material in front of the calorimeter.

[8]Even measures using the double-angle technique (equation 15) clearly fail at very small $y$ since the direction of the scattered hadronic system, $\gamma$, cannot be measured if there is little or no hadronic energy.



| Selection | H1 | ZEUS |
|---|---|---|
| Electron Angle | $160 - 172.5°$ | $3 - 173°$ |
| Electron Energy | $> 10.4\ GeV$ | $> 5\ GeV$ |
| $\sum(E - p_z)$ | $> 30\ GeV$ | $> 35\ GeV$ |
| $y_e$ | $< 0.6$ | $< .95$ |
| $y_h$ | $> .06$[9] | $> .04$ |
| Final Sample | 1026 *evts* | 1299 *evts* |
| $\int \mathcal{L} dt$ | $22.5\ nb^{-1}$ | $24.7\ nb^{-1}$ |

Table 5: *Selections and sample sizes for the 1992 published data from HERA. The rationale for the various cuts is discussed in the text.*

Table 5 summarizes the selections made in the two experiments. Though the variables are essentially the same, there are differences in the cut values on the minimum electron energy; the electron fiducial regions [within 20° of the electron beam direction by H1 and over the full solid angle by ZEUS]; the upper $y$-cuts [somewhat lower for H1]; and the lower $y$-cut [completely removes data of poor resolution in one case (ZEUS) while the H1 experiment utilizes data of poor $x$-resolution at low $y$ as described previously].

Figure 8 shows the regions in the $x - Q^2$ plane covered by the two sets of experimental selections. Superimposed are the bin centers for H1 and the bin outlines for ZEUS. The restriction by H1, $\theta > 160°$, limits their $Q^2$ range to below 100 $GeV^2$. The H1 experiment has also chosen to utilize the small $x$-region with $Q^2 < 10\ GeV^2$.

# 8 Structure Function Results

Selected events located within the appropriate bins of $x - Q^2$, together with the measured flux, determine the differential cross-sections in those bins. The

[9]Data below this cut are included but treated as a single $x$ bin. See text.

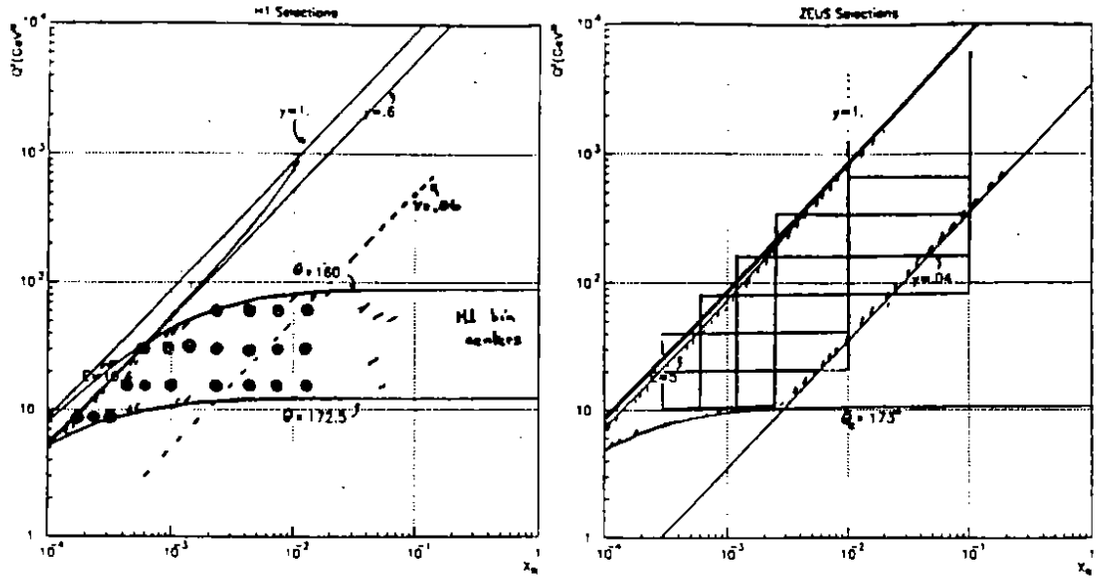


Figure 8: *Regions of $Q^2$ versus $x$ explored for the experimental selections described. The left plot shows the region and bin centers for the H1 collaboration; the right shows the bin outlines for the ZEUS group. (See text.)*

measures of $F_2(x, Q^2)$ are obtained from the cross-sections using the equation

$$\frac{d^2\sigma}{dx\ dQ^2} = \frac{2\pi\alpha^2}{xQ^4}\left[2(1-y) + \frac{y^2}{1+R}\right] F_2(x,Q^2)\{1+\delta_r(x,Q^2)\}$$

where

- $R$ is calculated from QCD and parameterized parton distributions;
- $\delta_r$, the radiative correction, is calculated from QED and parameterized parton distributions;
- the smearing, bin-centering, and similar corrections are performed in the usual manner.

Because the cuts and binnings are different, the two groups have some points which are unique and others which overlap. Figure 9a shows the



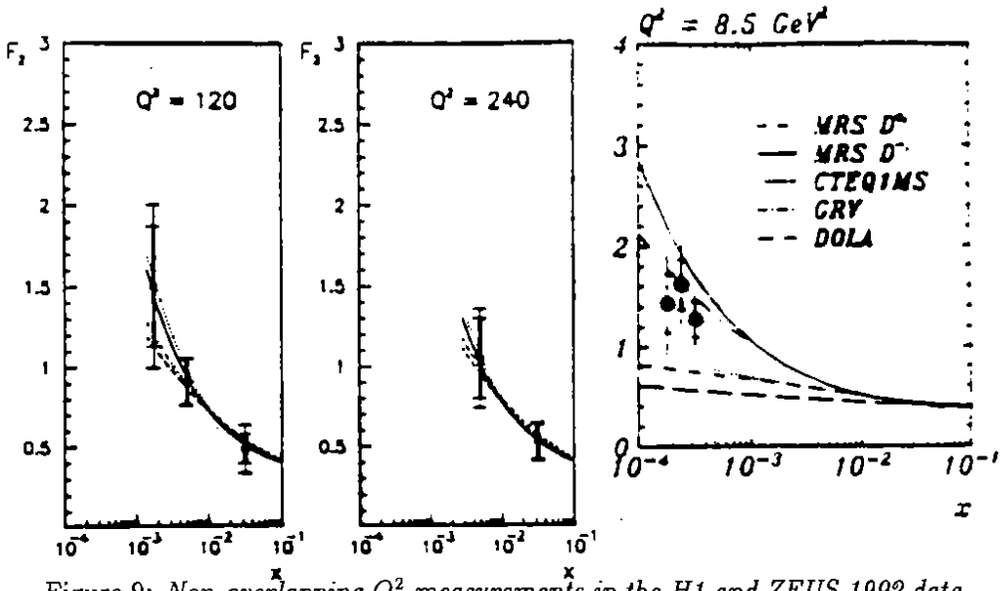


Figure 9: *Non-overlapping $Q^2$ measurements in the H1 and ZEUS 1992 data. The two left figures are from ZEUS; the right figure is from H1.*

data of H1 measured at $Q^2 = 8.5\ GeV^2$. Figures 9(b,c) show the structure functions obtained by ZEUS for $Q^2 = 120$ and 240 $GeV^2$, respectively. [Not shown are two ZEUS points with about 20% statistical accuracy at $Q^2 = 480$ and 1000 $GeV^2$.] Comparisons are superimposed on the data in these and the following figure of various parameterizations [41][42][43] of $F_2$ which differ primarily in the assumptions for the gluon and sea densities in the low $x$ region, as described earlier.

Figure 10 shows the H1 and ZEUS points in the bins with $Q^2 = 15$, 30 and 60 $GeV^2$, where data exist from both groups. [Several of the H1 points at high x have bin centers with $y < .06$.] The agreement among these data is generally good, with the H1 points lying higher but well within the flux normalization errors of 7% and 5% quoted by H1 and ZEUS, respectively. The experimental error bars are still too large to make a quantitative distinction among all the phenomenological postulates. One interesting general feature of all the data is that $F_2$ is large and falls rapidly at small $x$ for all $Q^2$.

Though some phenomenological guesses [those with rapidly falling gluon and sea densities] also show this feature, the behavior contrasts sharply with the fixed target data at somewhat larger $x$; those data have a more constant

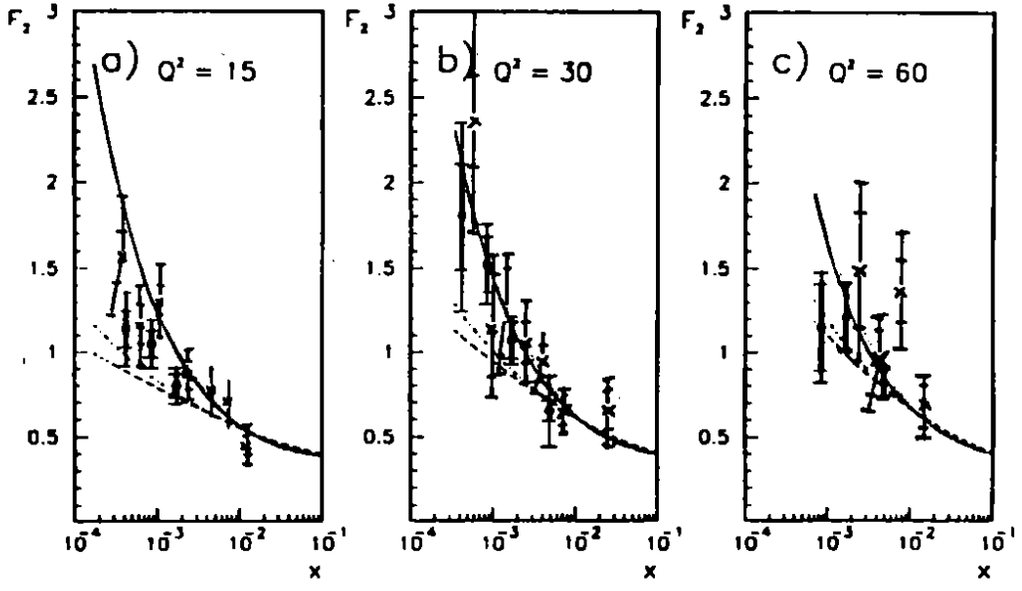


Figure 10: *Measurements at common $Q^2$ values by H1 (crosses) and ZEUS (dots) versus $x$ from the 1992 data. The phenomenological parameterizations are such that $MRSD_-$ and GRV are highest and largely indistinguishable; $MRSD_0$ lies lowest; and CTEQ lies just above $MRSD_0$*

dependence with $x > 0.01$ at similar values of $Q^2$. It is *very* interesting to see the qualitative features mirror those of the GRV predictions ( discussed earlier), which evolve from "valence-like" distributions at very small $Q^2$.

## 8.1 Gluon Density

The GLAP evolution equations, in leading order, predict [56] that the derivative of $F_2$ with $Q^2$ is proportional to a sum of integrals over $F_2$ and the gluon density, $G(x, Q^2)$. Assuming that the gluon term dominates this variation, a simple approximation has been derived [57], which provides a linear relationship between the derivative at $x$ and the gluon distribution evaluated at $2x$:

$$\frac{\partial F_2(x,Q^2)}{\partial \ln Q^2} \simeq \frac{10\alpha_s(Q^2)}{27\pi}\, G(2x,Q^2) \qquad (16)$$



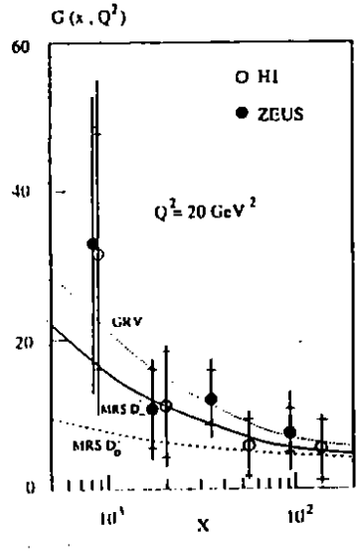


Figure 11: *Gluon distribution values extracted from the derivatives of the $F_2$ structure functions by H1 (open) and ZEUS (filled).*

It has been estimated [58] that this relation is accurate at the 20% level under the following assumptions:

- $\alpha_s$ is evaluated in leading order, using $\Lambda = 200\ MeV$,
- $N_f$ , the number of flavors, is taken equal to 4;
- the momentum transfer taken to evaluate this expression is taken at $Q_0^2 = 20\ GeV^2$.

The derivatives have been obtained from two data sets[58][59]. It should be noted that the H1 data bracket $Q_0^2$ , while the ZEUS data are at typically higher $Q^2$. Implicit in the use of equation (16) is the assumption that the logarithmic derivative does not change too quickly with $Q^2$.

The gluon distribution extracted from these points is shown in figure 11. The agreement among the points is remarkable, considering that the statistical (inner) error bars alone are enormous. The various phenomenological estimates are superimposed. This early initial data hints a tantalizing strong increase in $G(x)$ as $x \to 0$ that is similar to the behavior of the sea dominating $F_2(x)$.

# 9 Rapidity Gap Events

In the traditional picture that has evolved for lepton-nucleon scattering in the deep inelastic regime, a high momentum transfer virtual boson interacts with a point-like quark which proceeds to leave the vicinity of the nucleon remnant. Since both the quark and the proton remnant have net color, final state QCD processes must "dress" both the quark and the remnant, resulting in a substantial number of hadrons in the direction of each, as well as hadrons in the angular (or rapidity) interval between these two directions. This qualitative picture works in a large fraction of DIS processes at HERA [60]. This past year has seen the isolation of a number of events in which there is *no* energy visible either near the proton beam nor in the rapidity interval between the proton beam and the struck quark direction. Initially observed by the ZEUS collaboration [61], the phenomenon has been corroborated by H1 [47].

These "rapidity gap" events constitute about 5 $-10\%$ of the deep inelastic sample with $Q^2 > 10\ GeV^2$. [This means that there are fewer than one hundred events in each group's 1992 sample.] The simplest explanation for such a phenomenon would postulate a colorless system knocked from the proton. But the most obvious colorless systems are bound states of quarks and gluons. The probability of a bound system being ejected intact from the proton must fall with $Q^2$ , or be "higher twist" in QCD language. The evidence from the initial samples indicated that the fraction of such events does *not* fall rapidly. The newer ZEUS data presented at this conference [49], shown in figure 12, demonstrates with high statistical precision that the fraction of these events is essentially independent of $Q^2$ in three different regions of $x$.

An alternative explanation exists; indeed, there were those who anticipated that such events *should* occur[62]. The picture is that the virtual boson propagator which virtually dissociates into all fermion pairs may remain a quark pair if enough energy-momentum is transferred from the proton by a strong interaction to keep the final state on the mass shell. This is most likely a diffractive mechanism or, in Regge terminology, through exchange of a Pomeron. Alternatively, the boson interacts with a quark within the Pomeron. Though this mechanism will not obviously make a collimated hadronic jet, it will produce a configuration of final state hadrons unlike the "typical" DIS case.



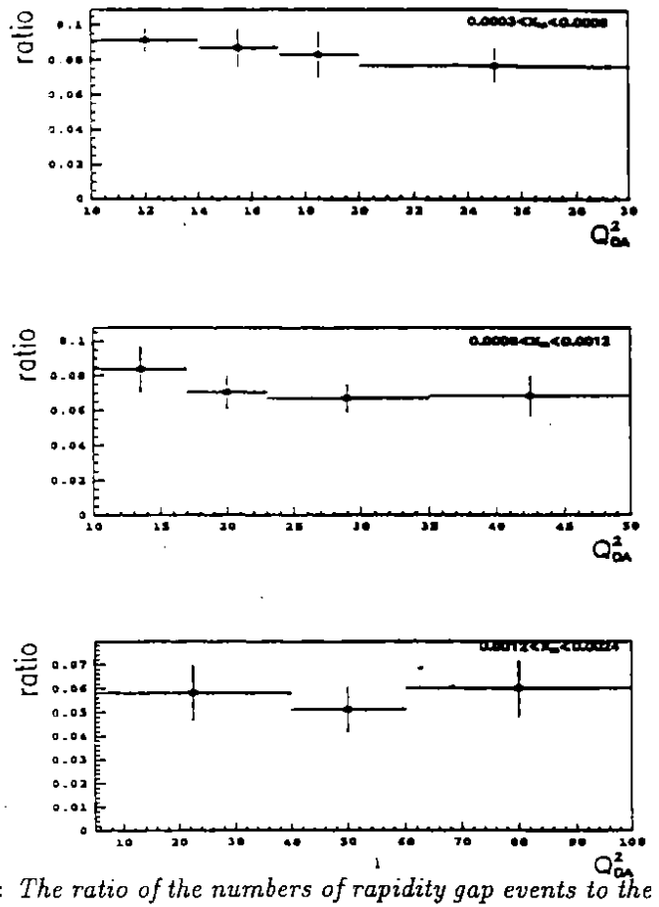


Figure 12: *The ratio of the numbers of rapidity gap events to the total number of DIS events versus $Q^2$ in ZEUS 1993 data. Three ranges of $x$ are shown:* .0003 *to* .0006 *(top);* .0006 *to* .0012 *(middle); and,* .0012 *to* .0024 *(bottom).*

The H1 group gave a taste of these explanations at this meeting [50], with comparisons against their 1993 rapidity gap data shown in figure 13 of two hypotheses for fitting at the larger rapidity gaps. Figure 13a superimposes a calculation with a vector dominance model to describe photon dissociation; figure 13b provides a "rapgap" model employing estimates of the pomeron flux and quark constituency. Some linear combination of these two models are likely to fit the observations. The 1993 data from both groups is eagerly awaited to help flesh out the mechanisms underlying these events.

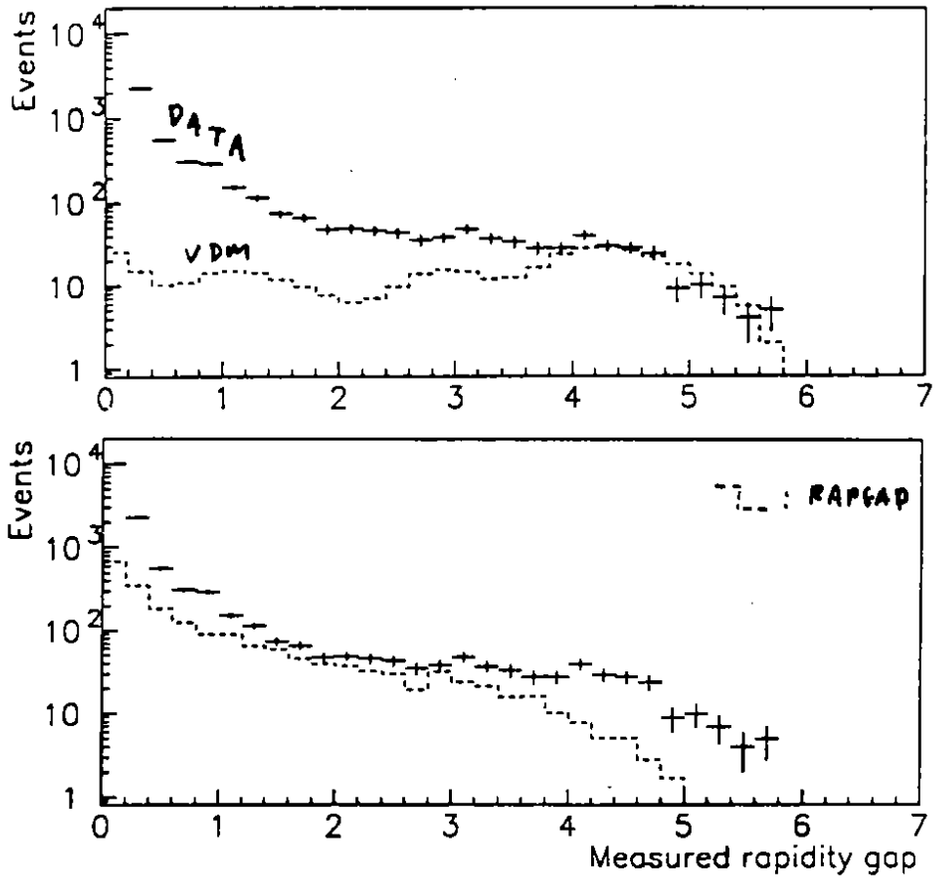


Figure 13: *H1 1993 data showing the rapidity relative to the detector edge with two hypotheses: VDM, with the photon dissociation into quarks (top); and "rapgap", involving scattering from quark constituents of the Pomeron (bottom).*

There was an interesting presentation [63] at this workshop of events observed by the $D^0$ collaboration at the Fermilab collider. These events, containing two very large transverse momentum jets, are typical *except* that that there is little or no hadronic activity observed between the two jets. There *are* hadrons between each jet and the nearest proton (or antiproton) remnant, however. Such events are also likely to be caused by exchange of a colorless object, but they would appear to lie in a much higher regime of momentum transfer for the exchanged "Pomeron" than typical of the rapidity



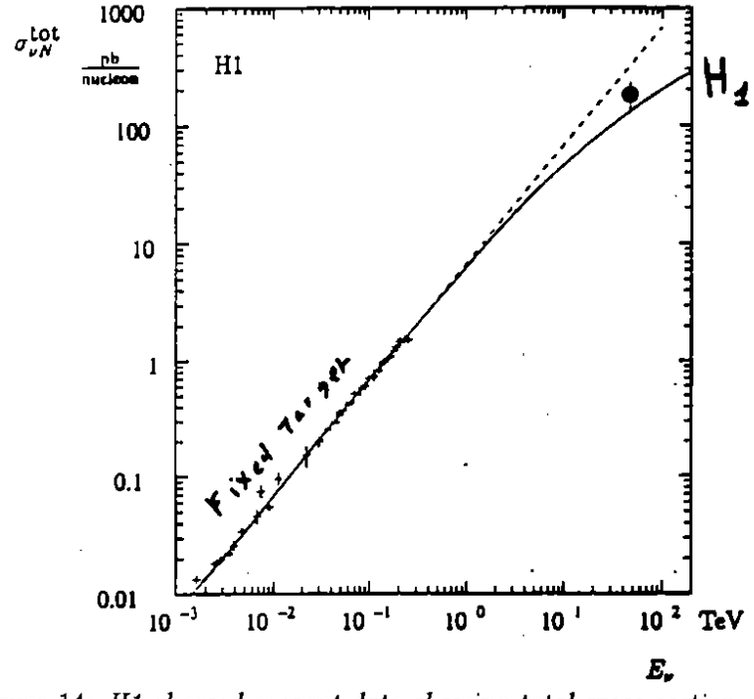


Figure 14: *H1 charged current data showing total cross-section versus equivalent fixed target neutrino energy, $E_\nu$.*

gap events from HERA. If there is a common or related origin for these events, hadronic colliders may provide a welcome complementarity to high statistics HERA data.

# 10 High $Q^2$ Results

Presentations at this meeting of 1993 high $Q^2$ data was exciting. Figure 14 shows the charged current total cross-section from H1 [50], compared with neutrino fixed target data, versus equivalent neutrino energy. These demonstrate beautifully the damping by the $W$-propagator at equivalent neutrino energies two orders of magnitude higher than previously measured. The ZEUS neutral current and charged current differential cross sections versus $Q^2$ are shown [49] in figure 15. In both cases the data agree with expectations, shown as smooth curves, up to $Q^2$ exceeding $10^4$ $GeV^2$. Higher luminosities will be very welcome to provide serious checks of electroweak

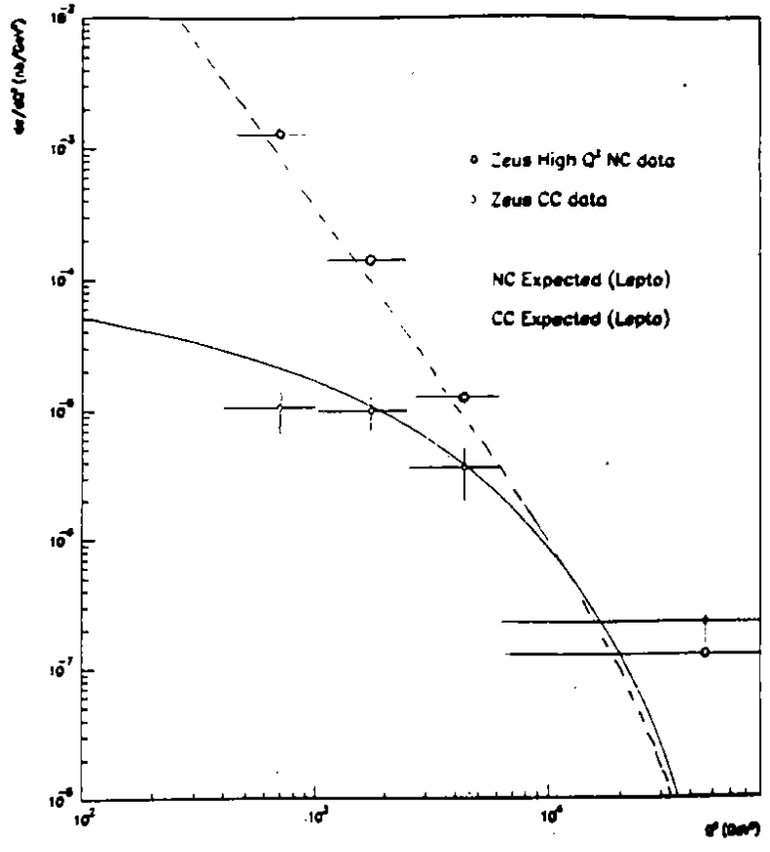


Figure 15: *High $Q^2$ 1993 data on neutral and charged current processes from the ZEUS experiment. The expected dependence is shown as smooth curves.*

theory and QCD in the regime of high momentum transfers and large center-of-mass energies.

# 11 Theoretical Developments

This workshop has been personally satisfying to me because I have learned much about theoretical developments in structure functions, particularly at small $x$, that have been taking place over the past several years. Though I cannot claim to have yet fully understood all these, much less to be able to anticipate what will be done, it is clear to me that we experimentalists very much need these new ideas. Lets review where we are.



## 11.1 GLAP Evolution

Sincere thanks are due to the originators of the QCD perturbative evolution equations [3] and to the phenomenological estimates [41][42][43] of low $x$ parton densities. The fixed target program has resulted in demonstrations that these evolution equations work well experimentally with non-singlet quark distributions, and also have produced a rather complete set of parton densities at $x > 10^{-2}$. Are these issues to be pursued in the same way for the new low $x$ regime of HERA? There are several reasons why this will be difficult.

1. The GLAP evolution *must* fail at some point due to saturation of parton densities.

2. If some evidence for GLAP breakdown appears the issue will be confused by possibilities for "higher twist"; these must be reconciled before we can say that we have *demonstrated* that GLAP must be modified.

3. The use of non-singlet distributions to *demonstrate* GLAP validity (or breakdown) is arguably difficult (impossible) at HERA, unless much higher luminosities are achieved than are even contemplated at present.

4. The use of singlet distributions has the complication that there is the additional freedom of an unknown gluon distribution. Can we really unravel whether GLAP is failing, whether higher twist is required, or whether a few more parameters might fix the problem?

At the very least, we will need to measure the gluon distribution in several different ways to assure ourselves that we are making a reproducible measurement of an objectively observable physical process. In any event, I have little doubt that we need more than the traditional GLAP evolution to interpret what is going on at small $x$.

## 11.2 Parton Model and Regge Predictions

The parton model, which expresses the conclusions of leading order in perturbative QCD, anticipates that the Regge description of the total photon-proton cross section should carry over to the description of the power-law dependence on $x$ of the $F_2$ structure function[33]. This description works well for fixed target data [64] with $Q^2 < 10\ GeV^2$, and we might well expect

this description to continue to even smaller $x$ unless some new physics mechanisms come into play. Straightforward extrapolations of fixed target data, using such techniques, predict [33]

$$F_2^{pred}(x = .001, Q^2 \sim 10\ GeV^2) \approx 0.5$$

and with locally flat dependence on both $x$ and $Q^2$. A glance at figures 9 and 10 demonstrates that the measured values at this value of $x$ and in this general regime of $Q^2$ is at least *twice* this large and increasing *rapidly* as $x$ becomes smaller. In this view, the data are indicating that some new physics principles are coming into play.

Indeed, we noted earlier that the general qualitative features of the data are reproduced in the GRV calculation [43], which begins with only "valence-like" distributions of valence, sea, and gluons at very low momentum transfers. Though this specific picture is perhaps not terribly attractive, the feature of a very soft (in $x$) parton distribution at high $Q^2$ is a general one that follows from GLAP evolution even with the hardest distributions at low $Q^2$ [65], and so prompts us to think that perhaps the low $x$ behavior of structure functions may be calculable from very general principles. Indeed, there has been work along precisely these lines for the past several years.

## 11.3 New Approaches at Small $x$

New approaches to the problem of small $x$ constituency of hadrons have been very productive. Some time ago, it was demonstrated [66] that perturbative QCD dictates a rapid rise as $x$ approaches zero. Later efforts succeeded in summing all terms at each order of the perturbative expansion which have the highest powers of $\ln(1/x)$ to produce an equation (Lipatov or BFKL equation) [67] satisfied by the gluon distribution at small $x$ involving only the quark-gluon coupling, $\alpha_s$. With simplifying assumptions, solutions to this equation provide gluon distributions that have a power law behavior, $g(x, Q^2) \sim x^{-\lambda}$. Indeed, there is even a rough prediction for this power

$$\lambda = \frac{12 \ln 2}{\pi} \overline{\alpha}_s$$

where $\overline{\alpha}_s$ is a parameter representing the running coupling, $\alpha_s$, taken as constant for the calculation. The exponent can take on large values, $\lambda \sim \frac{1}{2}$. If



the sea follows the gluon distribution, we have anticipated a substantial power law falloff of the structure function at small $x$. There have been sophisticated treatments of these issues, which unite [68] the BFKL equation with the GLAP evolution (called the Marchesini or double leading log approximation, DLLA, equation). Furthermore, there are expected to be saturation effects at sufficiently small values of $x$ that provide us with the GLR equation[69]. Developments were discussed by many of the participants at this workshop.

These approaches are very clearly of critical importance. Experimentalists require some realistic guidance beyond GLAP for comparing their data to hypotheses. We need clear expositions of these various approaches, with parameterizations that delineate clearly when a particular approach is or is not working with data.

## 11.4 What is HERA missing?

It is important to understand whether the HERA experiments are and will be optimized for unraveling various mysteries of the universe, and particularly for this workshop: those of QCD.

Probing the new regime of high $Q^2$ will require that HERA achieve design luminosity, which we have all taken to mean a yearly luminosity accruement of $\int \mathcal{L} dt = 100\ pb^{-1}$. It is essential that HERA get there as quickly as possible.

But, we are already hurt at accessible momentum transfers by a missing decade of $x$ between where we measure well and where fixed target experiments begin ( $.003 < x < .03$ ). The new structure functions of HERA, plotted versus $x$, would demonstrate new physics with so much more clarity if we could see the dramatic shift from a rapidly falling spectrum to an almost flat spectrum in a single experiment. Extensions of the $x$ range for HERA experiments should be given thought.

An estimate for where the gluon density becomes so large that partons overlap [65] is

$$xG(x, Q^2) \geq \frac{1\ fm^2}{1/Q^2} \approx 25\ Q^2(GeV^2)$$

The data of figure 11, with $Q^2 = 20\ GeV^2$, are clearly smaller than this. But we expect that the gluon density changes only logarithmically with $Q^2$; if so, then this bound may well be exceeded at lower $Q^2$. We must consider the

possibility that effects of saturation may well be observable in the small $x$ regime if we could reach lower, at least to the traditional "scaling" region, $Q^2 \sim 1\ GeV^2$.

Indeed, we should think hard for many reasons about extending our measurements to lower momentum transfers. Can one ever legitimately say that we have an understood theory of strong interactions when we have no viable method for predicting the results of experiments in the "normal" world, that is at low $Q^2$? I believe that such understanding is essential, and therefore in the longer term inevitable. Measurements at low $Q^2$ are desirable; it will require thought how best to achieve them.

Will one ever be able to measure accurately a nonsinglet, or valence-like, parton density at HERA? There is no chance of doing this without the high statistical precision which will only be brought with high luminosities. Can one ever measure a flavor distribution? Should one use the beautiful potential flexibilities of HERA for these and other purposes, including search for all the possibilities that lie beyond the Standard Model and beyond this workshop? There are unique sensitivities obtainable by replacing protons with deuterons, positrons with electrons, polarization for the initial electrons, and any combination of these. Should they be used? Any will require high luminosity and flexible operation of the HERA collider.

# 12 Conclusions

After concluding that the theorists should solve QCD completely, and the machine experts should provide an eminently flexible and highly luminous HERA, what is left for the experimenters? Indeed, they must think about what they need to measure and how best to do it. There are many choices to be made, because one will not be able to do it all. I claim no special insight into this question but as an experimenter, I have an opinion: the analysis of 5 $pb^{-1}$ could be a study in frustration. Though such a sample is an order-of-magnitude more than exists, it will not yet be adequate to separate $R$, whose magnitude will begin to be important. It will also not yet be adequate to separate the gluon distribution without facing up to large systematic errors. It is unlikely that any of these issues will be resolved without a very good plan, flexible modes of operation, and high luminosity.

HERA physicists are faced with problems not unlike those described by Andrzej Wróblewski at last night's dinner, in his description of Rothstein's intelligent *Wiggleworms*. These clever creatures, whose sensory experience has developed along a completely different route from our own, evolved at the bottom of a sea in a world of "muck". Living in their murky world, they have become technologically sophisticated without ever having seen the sky. Clearly, their physics would be completely different from our own. If in time, a particularly imaginative worm manages to invent a balloon and a telescope, he would only have to rise to the top of the muck and sea, point the telescope up, and he would see the grandeur and glory of the astronomical universe. Surely this would revise his science in a wonderful and glorious way!

Like our wiggleworm, we have wonderful new instruments, HERA and her detectors. Like our worm, perhaps, there is a new world to be discovered. Now all we need to answer is, "Which direction is the sky?"



# References


[1] M. Gell-Mann, **Phys. Lett. 8** (1964) 214; G. Zweig, 8182/TH 412 (1964) unpublished.

[2] G. Miller *et al*, **Phys. Rev. D5** (1972) 528; A. Bodek *et al*, **Phys. Rev. Lett. 30** (1973) 1087.

[3] V.N. Gribov and L.N. Lipatov, **Sov. J. Nucl. Phys. 15** (1972) 438; L.N. Lipatov, **Yad. Fiz. 20** (1974) 181; G. Altarelli and G. Parisi, **Nucl. Phys. B126** (1977) 298.

[4] S.R. Mishra and F. Sciulli, **Ann. Rev. Nucl. Part. Sci. 39** (1989) 259.

[5] W.C. Leung, "Nucleon Structure Functions from High Energy Neutrino-Iron Interactions at the Fermilab Tevatron", CCFR Collab, PhD Thesis Columbia University (1991), Nevis 276.

[6] G. Altarelli and G. Martinelli, **Nucl. Phys. B26** (1977) 298.

[7] E. Hughes, "Polarized Lepton-Nucleon Scattering", Proceedings of the 21st Annual SLAC Summer Institute on Particle Physics, Stanford, CA (1993), SLAC-PUB-6439.

[8] V. Hughes, Proceedings of this workshop.

[9] S. L. Adler, **Phys. Rev. 143** (1966) 1144.

[10] D. Allasia *et al*, BEBC Collab, **Phys. Lett. B135** (1984) 231; **Z. Phys. C28** (1985) 321.

[11] K. Gottfried, **Phys. Rev. Lett. 18** (1967) 1154.

[12] D.J. Gross and C. H. Llewellyn-Smith, **Nucl. Phys. B14** (1969) 337.

[13] J. D. Bjorken, **Phys. Rev. 148** (1966) 1467; **Phys. Rev D1** (1970) 1376.

[14] P. Amaudruz *et al*, NMC Collab, **Phys. Rev. Lett. 66** (1991) 2712; **Nucl. Phys. B371** (1992) 3.

[15] M. Arneodo *et al*, NMC Collab, "A Re-evaluation of $F_2^n/F_2^p$ and $F_2^p - F_2^n$ ", CERN-PPE/93-117 (July 1993); M. Arneodo *et al* (NMC Collab) **Phys. Lett. B309** (1993) 222.

[16] A. D. Martin *et al*, **Phys. Lett. B252** (1990) 653. V.R. Zoller, **Phys. Lett. B279** (1992) 145; **Z. Phys. C54** (1992) 425.

[17] E.J. Eichten, I. Hinchliffe, C. Quigg, **Phys. Rev. D45** (1992) 2269.

[18] R.D Field and R.P. Feynman, **Phys. Rev. D15** (1977) 2590.

[19] W.C. Leung *et al*, CCFR Collab, **Phys. Lett. B317** (1993) 655.

[20] S. A. Larin and J.A.M Vermasen, **Phys. Lett. B259** (1991) 345.

[21] J. Bjorken, private communication.

[22] J. Ashman, et al, **Phys. Lett. B206** (1988) 364; M.J. Alguard *et al*, **Phys. Rev. Lett. 37** (1976) 1261; G. Baum *et al*, **Phys. Rev. Lett. 51** (1983) 1135.

[23] P. L. Anthony *et al*, E142 Collab, **Phys. Rev. Lett. 71** (1993) 959; B. Adeva *et al*, SMC Collab, **Phys. Lett. B302** (1993) 533.

[24] H. Abramowicz *et al* (CDHS Collab) **Z. Phys C25** (1984) 29.



[25] J.P. Rutherfoord, **Proc. of the Workshop on Hadron Structure and Parton Distributions**, ed. by C.H. Albright *et al* , (April 1990) World Scientific, p. 234.

[26] A. Bodek, **Proc. of the Workshop on Hadron Structure and Parton Distributions**, ed. by C.H. Albright *et al* , (April 1990) World Scientific, p. 67.

[27] S.D. Ellis and W.J. Stirling, **Phys. Lett. 256B** (1991) 258.

[28] A.D. Martin, Proceedings of this workshop.

[29] W.-K. Tung, Proceedings of this workshop.

[30] M.A.G. Aivazis, F.I. Olness, and W.-K. Tung, "Leptoproduction of Heavy Quarks I", SMU-HEP/93-16, submitted to **Phys. Rev. D**; .M.A.G. Aivazis, J.C. Collins, F.I. Olness, and W.-K. Tung, "Leptoproduction of Heavy Quarks II", SMU-HEP/93-17; submitted to **Phys. Rev. D**; M.A.G. Aivazis, F.I. Olness, and W.-K. Tung, **Phys. Rev. Lett. 65** (1990) 2339.

[31] A. O. Bazarko *et al*, CCFR Collab, **Proceedings of the XXVIIIth Rencontre de Morion: QCD and High Energy Hadronic Interactions**, ed by J. Tran Thanh Van, Gif-sur-Yvette: Editions Frontieres, 1993; S.A. Rabinowitz *et al*, CCFR Collab, **Phys. Rev. Lett. 34** (1993) 134; C. Foudas *et al*, CCFR Collab, **Phys. Rev. Lett. 64** (1990) 1207.

[32] V. Barone *et al*, "Non Universality Effects in Structure Functions Probed in Neutrino and Muon Deep Inelastic Scattering" , preprint DFFT - 04/94; "Leptoproduction of Charm Revisited", preprint DFFT 72/93 (Jan 1993).

[33] A. Donnachie and P.V. Landshoff, **Z. Phys. C61** (1994) 139.

[34] A. Donnachie and P.V. Landshoff, **Phys. Lett. B207** (1988) 319.

[35] M. Clark *et al* (BFP Collab), **Phys. Rev. Lett. 45** (1980) 1465; J. J. Aubert *et al* (EMC Collab), **Nucl. Phys. B213** (1983) 31.

[36] John Ellis and Marek Karliner, "Spin Structure Functions", CERN-TH.7022/93, PANIC '93 (June 1993).

[37] J. Ellis and R.L. Jaffe, **Phys. Rev. D9** (1984) 1444.

[38] P.Z. Quintas *et al*, **Phys. Rev. Lett. 71** (1993) 1307.

[39] B. Badelek, **J. Phys. G: Nucl. Part. Phys. 19** (1993) 1509, and references therein; M. Arneodo *et al* (NMC Collab) **Phys. Lett. B309** (1993) 222.

[40] R.K. Ellis, **Proc. of the Workshop on Hadron Structure and Parton Distributions**, ed. by C.H. Albright *et al*, (April 1990) World Scientific, p. 167.

[41] A.D. Martin *et al*, MRS Collab, **Phys. Lett. 306B** (1993) 145.

[42] J. Botts *et al*, CTEQ Collab, **Phys. Lett. 304B** (1993) 159.

[43] M. Glück *et al*, GRV Collab, **Z. Phys. C48** (1990) 471; **Z. Phys. C53** (1992) 127; **Phys. Lett. 306B** (1993) 391.

[44] A.D. Martin, W.J. Stirling, and R.G.Roberts, **J. Phys. G: Nucl. Part. Phys. 19** (1993) 1429.

[45] M. Bonesini *et al* (WA70 Collab) **Z. Phys. C38** (1988) 371.

[46] D. P. Barber *et al*, *High Spin Polarization at the HERA Electron Storage Ring*, DESY preprint 93-038 (April 1993). D. P. Barber, et al, Nucl. Instr. Meth. A329 (1993) 79.

[47] I. Abt *et al* (H1 Collaboration), Nucl. Phys. B407 (1993) 515.

[48] M. Derrick *et al* (ZEUS Collaboration), Phys. Lett. 316B (1993) 412.

[49] G. Wolf, plenary presentation at this conference.

[50] J. Feltesse, plenary presentation at this conference.

[51] I. Abt *et al* (H1 Collaboration), Nucl. Phys. B396 (1993) 3.

M. Derrick *et al* (ZEUS Collaboration), Phys. Lett. 306B (1993) 173; Phys. Lett. 316B (1993) 207.



[52] See, for example, M. Derrick *et al* (ZEUS Collaboration), Phys. Lett. 316B (1993) 412; I. Abt *et al* (H1 Collaboration:), Phys. Lett. 314B (1993) 436.

[53] I. Abt *et al* (H1 Collaboration) *The H1 Detector at HERA*, DESY preprint 93-087 (1993).

[54] M. Derrick *et al* (ZEUS Collaboration), Phys. Lett. 303B (1993) 183.

[55] S. Bentvelsen, J. Engelen and P. Kooijman, *Proceedings of th Workshop 'Physics at HERA'* vol 3 (DESY,1992), 23.

F. Jacquet and A. Blondel, *Proceedings of the Study of an ep Facility for Europe* (DESY 79/48, 1979), 391.

[56] G. Altarelli and G. Martinelli, **Phys. Lett. 76B** (1978) 89; M. Glück and E. Reya, **Nucl. Phys. B145** (1978) 24.

[57] K. Prytz, Phys. Lett. 311B (1993) 286.

[58] I. Abt *et al* (H1 Collaboration), *Scaling Violations of the Proton Structure Function $F_2$ at Small $x$*, DESY preprint 93-146 (October 1993).

[59] M. Roco, *A Measurement of the Gluon Distribution at low-$x$ using $F_2(x,Q^2)$ Scaling Violations*, DESY ZEUS-note 93-088 (1993).

[60] T. Ahmed *et al* (H1 Collaboration), **Phys. Lett. 298B** (1993) 469.

M. Derrick *et al* (ZEUS Collaboration), **Z. Phys. C59** (1993) 231.

[61] M. Derrick *et al* (ZEUS Collaboration), **Phys. Lett. 315B** (1993) 481.

[62] G. Ingelman and P.E. Schlein, **Phys. Lett. 152B** (1985) 256.

[63] G. Forden, plenary presentation at this conference.

[64] P. Funaudrua *et al* (NMC Collab), **Phys. Lett B295** (1992) 159.

[65] A. H. Mueller, **J. Phys. G: Nucl. Part. Phys. 19** (1993) 1463.

[66] A. de Rujula *et al*, **Phys. Rev. D10** (1974) 1649.

[67] Y.Y. Balitsky and L.N. Lipatov, **Sov. J. Nucl. Phys. 28** (1978) 822; E. A. Kureav, L.N. Lipatov, and V. S. Fadin, **Sov. Phys.-JETP 45** (1977) 199.

[68] G. Marchesini, **Proc. Workshop 'QCD at 200 TeV'**, Erice (June 1990) NY, Plenum, p 183.

[69] L.V. Gribov, E.M. Levin, and A.G. Shuvaev, **Phys. Rep. 100** (1983) 1.